ELSEVIER

Tribology International 37 (2004) 679–687

TRIBOLOGY INTERNATIONAL

www.elsevier.com/locate/triboint

Dynamic characteristics of a flexible rotor system supported by a viscoelastic foil bearing (VEFB)

Yong-Bok Lee [a,*], Tae-Ho Kim [a], Chang-Ho Kim [a], Nam-Soo Lee [b], Dong-Hoon Choi [b]

[a] *Tribology Research Center, Korea Institute of Science and Technology, P.O. Box 131, Cheongryang, Seoul, South Korea*
[b] *Dept. of Mechanical Design and Production Engineering, Hanyang University, 17 Haengdang-dong, Seongdong-Gu, Seoul, South Korea*

Received 16 April 2002; received in revised form 16 January 2003; accepted 27 January 2003

Abstract

Foil bearings have been considered as an alternative to traditional bearings with the increasing need for high-speed, high-temperature turbomachinery. However, the lack of adequate load capacity and sufficient damping capacity is a key technical hurdle to super-bending-critical operation as well as widespread use of foil bearings in turbomachinery such as turbopumps, turbocompressors and turbochargers. A new foil bearing, ViscoElastic Foil Bearing (VEFB) is suggested in this paper. The super-bending-critical operation of the conventional bump foil bearing and the VEFB is examined, as well as the structural dynamic characteristics. The structural dynamic test results show that the equivalent viscous damping of the VEFB is much larger than that of the bump bearing and that the structural dynamic stiffness of the VEFB is comparable or larger than that of the bump bearing. The results of super-bending-critical operation of the VEFB indicate that the enhanced structural damping of the viscoelastic foil dramatically reduces the vibration near the bending critical speed. With the help of increased damping resulting from the viscoelasticity, suppression of the nonsynchronous orbit is possible beyond the bending critical speed.

Keywords: Viscoelastic foil bearing (VEFB); Bump bearing; Super-bending-critical operation; Structural dynamic coefficient; Viscoelasticity

1. Introduction

Super-bending-critical operation of turbomachinery is one of the meritorious features to open new avenues for the development of advanced rotating machinery. When it comes to the turbomachinery operated beyond the bending mode, it is possible to raise energy density, increase efficiency, and reduce rotor weight. But without superior rotordynamic characteristics, operation beyond the bending critical speed is not possible and this ability is beyond the capacity of conventional bearings.

A foil bearing which is a self-acting compliant-surface hydrodynamic bearing is a promising candidate for advanced rotating machinery. As the foil bearing surface is compliant, there are certain advantages such as lower power loss, better stability, and tolerance of a large foreign particle. The compliance of foil bearings also makes them more tolerant of centrifugal/thermal growth since the compliant foils can accommodate these changes in shaft diameter and bearing clearance due to the foil deflection [1]. In spite of the high potential of foil bearings, lack of adequate load capacity and sufficient damping capacity is a key technical hurdle to super-bending-critical operation as well as widespread use of foil bearings in turbomachinery systems such as gas turbine engines [2]. To overcome these shortages, various configurations of foil bearings have been developed by many investigators and the load capacity of foil bearings has increased more than double that demonstrated a decade earlier [3].

In terms of developing the advanced rotating machinery in the future, another new foil bearing, the ViscoElastic Foil Bearing (VEFB), is suggested. It consists of the viscoelastic top foil supported by a series of bump foils. This VEFB has the ability to operate beyond the bending critical speed and has the superior rotordynamic characteristics, higher damping and comparable stiffness

* Corresponding author. Tel.: +82-2-958-5663; fax: +82-2-958-5659
E-mail address: lyb@kist.re.kr (Y.-B. Lee).

0301-679X/$ - see front matter © 2003 Published by Elsevier Ltd.
doi:10.1016/S0301-679X(03)00013-6

Nomenclature

C_{mn}	damping coefficients; $m,n=x$ or y
C'_{mn}	non-dimensional damping coefficients; $m,n=x$ or y; $C'_{mn}=C_{mn}c\omega/P_aR^2$
C^{BB}	damping of the bump bearing
C^{VB}	damping of the viscoelastic bearing
c	radial clearance
K_{mn}	stiffness coefficients; $m,n=x$ or y
K'_{mn}	non-dimensional stiffness coefficients; $m,n=x$ or y; $K'_{mn}=K_{mn}c/P_aR^2$
K^{BB}	stiffness of the bump bearing
K^{VB}	stiffness of the viscoelastic bearing
P_a	ambient pressure
R	bearing radius
δ	dynamic amplitude
ΔC	damping ratio
ΔK	stiffness ratio
ω	rotating speed

compared with the bump foil bearing. To demonstrate the superior characteristics, super-bending-critical operation of the conventional bump foil bearing and the VEFB is examined, as well as the structural dynamic characteristics. In both tests, structural damping, vibration orbit, and the modal damping ratio of the bump and viscoelastic bearings were compared.

2. Experimental apparatus

In this section, a new foil bearing, ViscoElastic Foil Bearing (VEFB), is suggested. In addition, the damping mechanism of the VEFB is explained in detail. The experimental set-ups for the structural dynamic and super-critical operation tests are carefully explained. The results for the structural dynamic test are also given.

2.1. Schematics of the viscoelastic foil bearing

As shown Fig. 1, the ViscoElastic Foil Bearing (VEFB) consists of a smooth top foil, a viscoelastic foil, and a bump foil. The smooth single top foil is made of SUS 301 and is heat-treated before it is installed. It is 35 mm wide and extended to about 355 deg in the circumferential direction, forming the equivalent of a full bearing. The viscoelastic foil is made of acrylic viscoelastic polymers and withstands temperatures as high as 150°C. The shim is made of the same material as the top foil and is inserted between the bump foil and the bearing housing to prevent housing surface damage. The bump foil is fixed to the bearing housing after it is formed. The upper surface of the viscoelastic foil is adhered to the back of the top foil and the lower surface adhered to the upper surface of the bump foil. It is expected that the viscoelastic foil will increase the damping of this bearing since the viscous portion of the viscoelastic foil dissipates the energy during any type of deformation. In addition to the viscoelastic damping of the VEFB, the rubbing surfaces of bump foils are sputter coated with copper to improve frictional characteristics between the bump foil and the shim foil. The top foil of the bearing is coated with molybdenum disulfide (MoS_2) on the side that mates with the journal to reduce start–stop wear and friction.

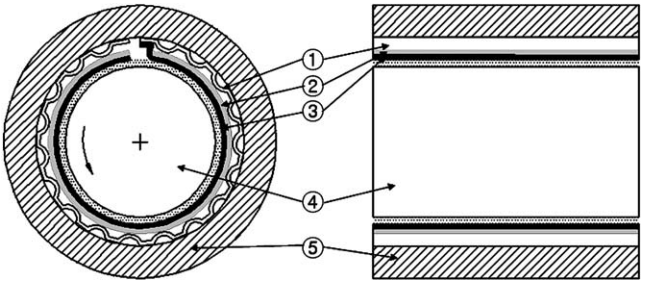

Fig. 1. Viscoelastic foil bearing: (1) bump foil, (2) viscoelastic foil, (3) top foil, (4) shaft, (5) sleeve.

Fig. 2 and Table 1 present a schematic diagram and pertinent dimensional information of the VEFB, respectively. With hydrodynamic pressure placed on the surface of the top foil, the damping force is generated because the viscoelastic polymer material under the top foil dissipates the energy. In addition, total structural damping and stiffness forces develop in some combinations with the bump and viscoelastic foils.

2.2. Experimental set-up for the structural dynamic test of foil bearings using shakers

A test facility shown in Fig. 3 is built to investigate the structural dynamic characteristics of the viscoelastic

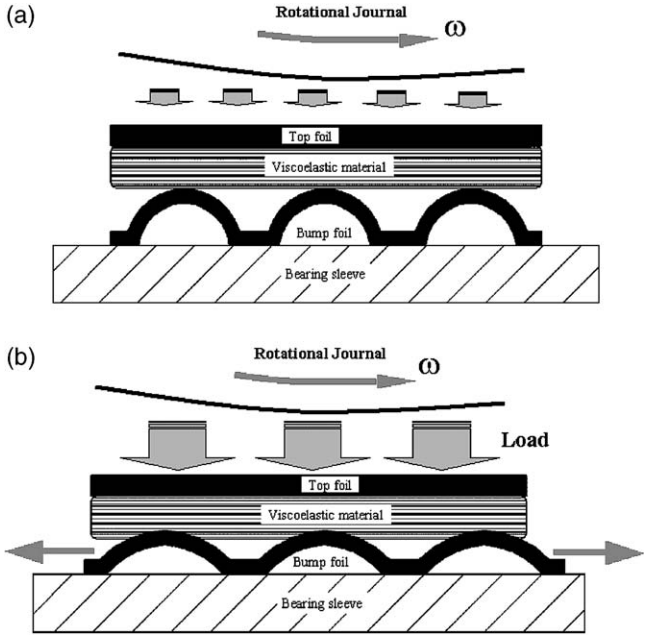

Fig. 2. Schematic diagram of the VEFB: (a) unloaded configuration, (b) loaded configuration.

Table 1
Viscoelastic foil bearing configuration

Bearing length, mm	35
Bearing diameter, mm	35.45
Approximate running diametral clearance, mm	0.05~0.07
No. of pad	1
Top foil:	
Foil thickness, mm	0.12
Foil radius, mm	20
Foil material	SUS301
Foil coating	MoS_2
Bump foil:	
Bump pitch, mm	3.1
Bump length, mm	2.6
Bump height, mm	0.45
No. of bumps	1
Foil thickness, mm	0.1
Foil material	SUS301
Foil coating	copper
Viscoelastic foil:	
Foil material	acrylic polymer
Foil thickness, mm	0.1

bearing and the bump foil bearing. The viscoelastic bearing and the bump foil bearing are identical except that the bump bearing does not have the viscoelastic foil. The rotor with a diameter of 60 mm is supported by two deep groove ball bearings. The test bearing is floated around the center portion of the shaft. The inner diameter of the test bearing is 61.45 mm with a length of 60 mm and a dead weight of 5.3 kg. Four displacement probes, with a sensitivity of 78.7 V/mm, are used to measure the displacement of the bearing housing at both ends in the horizontal and vertical direction. Four accelerometers, with a sensitivity of 101.1 mV/g, are used to measure the acceleration of each ball bearing housing in the horizontal and vertical directions. The force transducer, with a sensitivity of 22.91 mV/N, is attached to the outer surface of the bearing housing at the center location in the transverse direction on one end, while it is fixed on the stinger of the electromagnetic shakers on the other end. The test bearings are excited by two electromagnetic shakers, which are 90 degrees apart. It should be noted that the exciters are offset 45 degrees from vertical and horizontal directions as shown in Fig. 3 because of a limitation of space. Therefore, a coordinate transformation is performed before the structural dynamic coefficients of the bearings are calculated. Two oscilloscopes are used to monitor the displacement of the test bearing and ensure that the test bearing translates, i.e. not declines, in the horizontal and vertical direction. The FFT Signal Analyzer is used to identify the amplitude and the phase of the test bearing displacement and the exciting force. All the outputs of the probes and the transducers are recorded for post-process and analysis.

2.3. Results for the structural dynamic test of the bump foil bearing and the VEFB

The structural dynamic tests are performed to investigate the structural dynamic characteristics of the viscoelastic bearing and the bump foil bearing. The dynamic tests are conducted at 5.3 kg_f (bearing dead weight). At bearing static load, four dynamic amplitudes of 1.0 to 2.5 mm were tested at 150, 200, and 250 Hz. The dynamic structural stiffness and the equivalent viscous damping of each bearing were calculated by the structural dynamic equations, which describe the relationships between the applied dynamic forces and the structural dynamic coefficients. These structural dynamic equations, which are virtually identical with those of Heshmat [4], are presented in Appendix A.

The structural dynamic coefficients of the bump foil bearing and the VEFB are compared in Fig. 4(a) and (b). The variables are defined in the Nomenclature. In Fig. 4(a), *Cxx* of the VEFB is much larger than *Cxx* of the bump bearing while *Cyy* of the VEFB is smaller than *Cyy* of the bump bearing. It is noted that *Cxx* has a dominant effect on reducing the vibration amplitude because the static bearing load is applied in the vertical direction. The direct terms, *Cxx* and *Cyy*, decrease with the increasing dynamic amplitude although the energy dissipation increases. The cross-coupling terms, *Cxy* and *Cyx*, are much smaller than the direct terms, *Cxx* and *Cyy*, which are the characteristics of the structural dynamic test. Fig. 4(b) presents the dynamic stiffness coefficients of both bearings. *Kxx* of the VEFB is larger than *Kxx* of the bump bearing while *Kyy* of the VEFB is smaller than *Kyy* of the bump bearing. i is much larger than i,

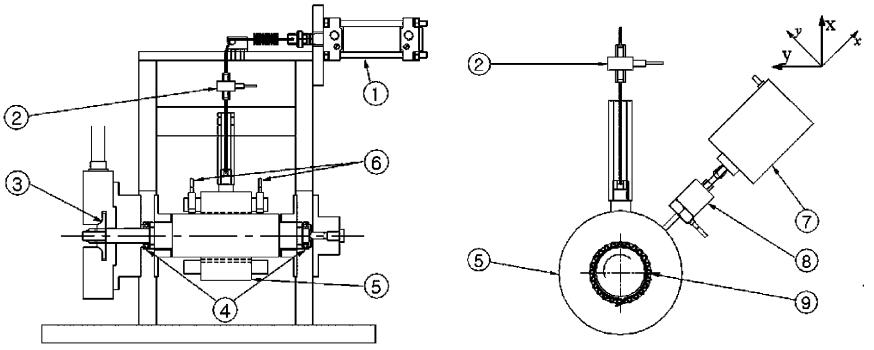

Fig. 3. Structural dynamic test apparatus: (1) air cylinder, (2) load cell, (3) air turbine, (4) ball bearings, (5) test foil bearing sleeve, (6) gap sensors, (7) shaker, (8) force transducer and accelerometer, (9) test bump foils.

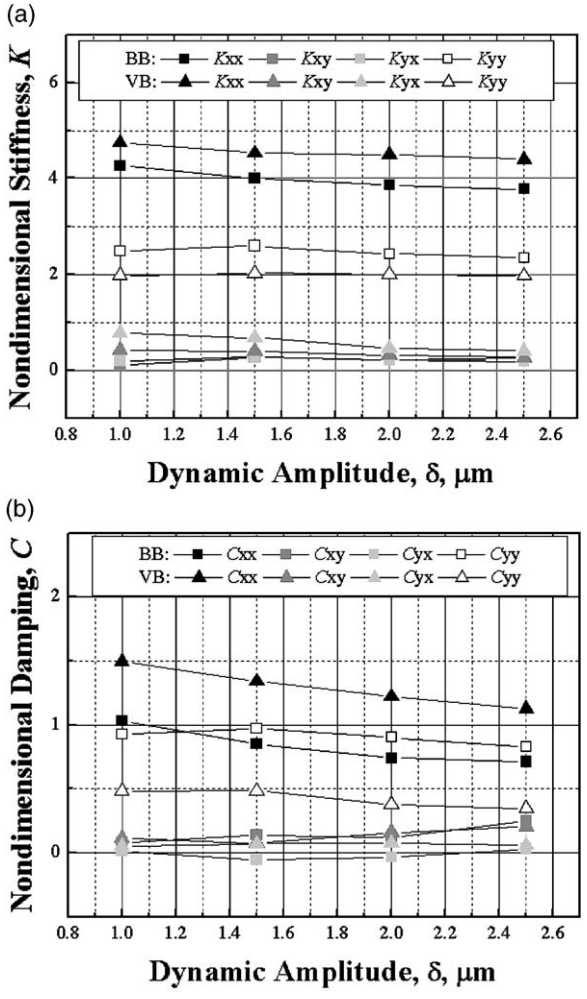

Fig. 4. Comparison of the structural dynamic coefficient between the BB and VB (BB: the bump foil bearing, VB: the viscoelastic bearing): (a) non-dimensional stiffness, (b) non-dimensional damping.

due to the fact that the static load is applied in the vertical direction. To elucidate the effect of the viscoelastic foil, the direct stiffness and damping ratio, defined as $\Delta K_{xx} = (K_{xx}^{VB} - K_{xx}^{BB})/K_{xx}^{BB}$, $\Delta C_{xx} = (C_{xx}^{VB} - C_{xx}^{BB})/C_{xx}^{BB}$, are shown in Fig. 5(a) and (b). The damping ratio is much larger than the stiffness ratio, which indicates that the viscoelastic foil enhances the damping more than the stiffness of the bearing. The damping ratio ranges from about 0.2 to 0.8 for a range of experiments. It can therefore be concluded that the equivalent viscous damping of the VEFB is much larger than that of the bump bearing and that the structural stiffness of the VEFB is comparable or larger than that of the bump bearing.

2.4. Experimental set-up for the foil bearing supported rotor beyond the bending critical speed

Fig. 6 shows a photo of the test apparatus. The bearings used in the super-critical operation test are the same as the bearings used in the structural dynamic test except for the diameter and the length of the bearings. The structural dynamic coefficients of the different-sized bearing can be evaluated using non-dimensional variables. The rotor with a mass of 5 kg, total length of 594 mm, and diameter of 35 mm has an integral impulsive-type air turbine at one end while the other end is free. The rotor is constrained axially by a pair of thrust buttons located at opposite ends of the shaft. The special tongue and groove pedestal arrangements are made to shift the location of the journal bearing along the shaft with ease. Three accelerometers, with a sensitivity of 100 mV/g, are used during the impact tests performed to place the journal bearings outboard of the free–free bending nodes. During the super-bending-critical operation of the foil bearings, six displacement probes, with a sensitivity of 7.87 V/mm, are used to measure the displacement of the shaft near the free end, the shaft axial center, and the impulsive turbine in the horizontal and vertical directions. The rotational speed of the shaft is measured using a remote optical probe, which responds to the once-per-revolution passing of a reflective tape stuck to the face of the shaft. Three oscilloscopes are used to investigate the orbits near the turbine end, the shaft axial center, and the free end. The FFT Signal Ana-

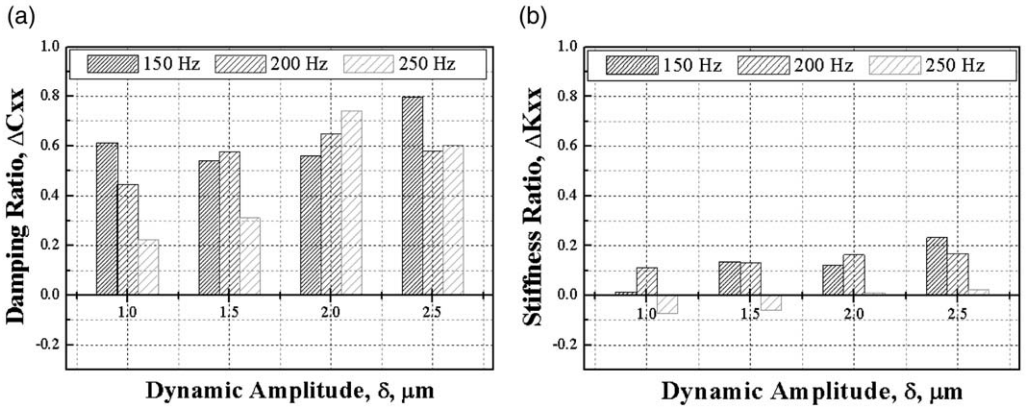

Fig. 5. Comparison of the structural dynamic coefficient ratio, (a) damping ratio, (b) stiffness ratio.

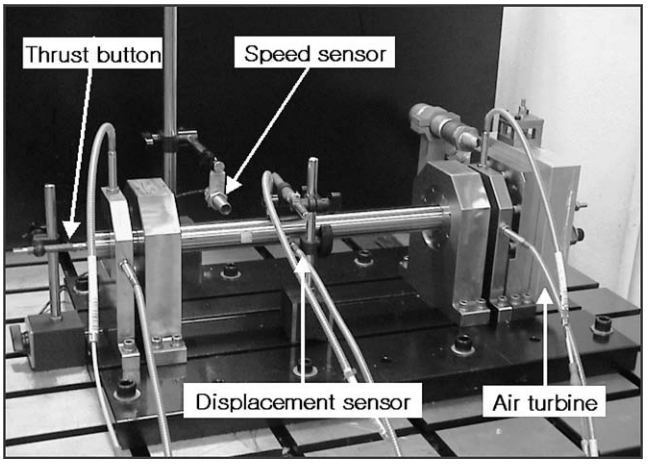

Fig. 6. The test apparatus.

lyzer is used to identify the critical speeds and to collect the vibration amplitude as a function of rotational speed. All probe outputs of the probes are recorded for post-process and analysis. During speed up operation, the vibration amplitudes are recorded to estimate bearing equivalent damping coefficients by the half power method.

3. Results for the foil bearing supported rotor beyond the bending critical speed

To find bending critical speeds and nodes of the rotor, impact tests are employed with the rotor suspended on monofilament cables and instrumented with three accelerometers. The first and second flexible mode frequencies are found to be 512 Hz and 1332 Hz, respectively. The nodes of first bending frequency are located at 171 and 471 cm from the turbine end. The rotordynamic analysis is performed based on a finite element program.

Fig. 7 shows the first two bending critical speeds and mode shapes. The first bending critical was predicted to occur at 526 Hz and the second critical at 1384 Hz. The prediction agrees well with the experimental result. The two journal bearings are located outboard of the free–free bending nodes while varying their positions. Fig. 8 shows the critical speed map, which is plotted as a function of bearing stiffness. For a range of the general foil bearing stiffness, the first two bending critical speeds are nearly constant since they are essentially unaffected by the soft supports such as the air bearings [5].

Figs 9 to 12 compare the orbits of the bump foil bearing with the VEFB at three different axial locations. Fig. 9 presents the orbits under the first bending critical speed. The vibration amplitude of the VEFB-supported rotor is comparable to the amplitude of the rotor supported by the bump bearings at all three locations (free end, the axial center, and the turbine). But near the first bending critical speed, 30,000 RPM, the vibration ampli-

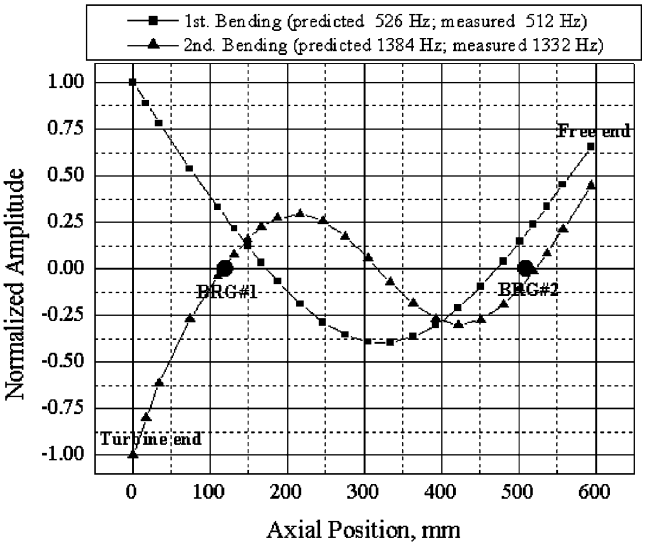

Fig. 7. The two free–free bending modes of the rotor.

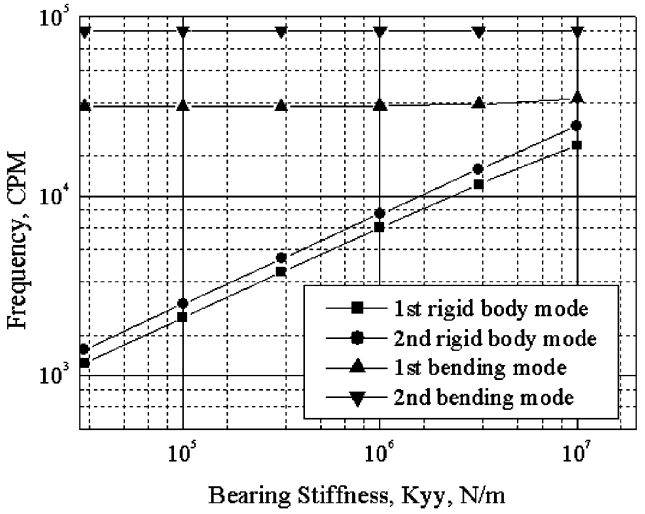

Fig. 8. Calculated critical speeds.

tude of the VEFB-supported rotor is reduced by as much as a factor of about four in the vertical direction, compared with the bump bearing as shown in Fig. 10(a). This indicates that the enhanced structural damping of the viscoelastic foil dramatically reduces the vibration near the bending critical speed because the viscous portion of the response dissipates the energy during any type of deformation of viscoelastic-type materials. At the axial center of the shaft, the vibration orbit in Fig. 10(b) exhibits a slightly different version of the "figure of eight" orbit, most likely due to a high degree of bearing film dynamic non-linearity associated with a high radial bearing [6,7]. Fig. 11 compares the orbits beyond the first bending critical speed, 40,000 RPM. The viscoelastic foil maintains its effect on reducing vibration. Fig. 12 shows the orbits at 50,000 RPM. The nonsynchronous orbit occurs at 50,000 RPM when the super-critical rotor is supported by the conventional bump bearings. This class of orbit likely occurs due to bump foil flexibility governing the stiffness of the compliant foil bearing. With the help of increased damping due to the viscoelasticity, suppression of the nonsynchronous orbit is possible as shown in Fig. 12.

Fig. 13 represents the comparison of order plot between the conventional bump bearing and the VEFB during speed-up. The increased damping of the VEFB retains the small maximum amplitude of rotor vibration at the first bending critical speed by as much as a factor of about two, when compared with that supported by the bump bearings. To estimate the damping capacity of each bearing, the modal damping ratio of each bearing is calculated by the half-power method. The modal damping ratio of the VEFB is 0.062 and that of the bump bearing 0.044. Assuming that the stiffness of the bump bearing and VEFB is equal, the damping ratio, ΔCxx is about 0.41. Considering that the average of the structural damping ratio at 250 Hz is 0.47, it is evident that the

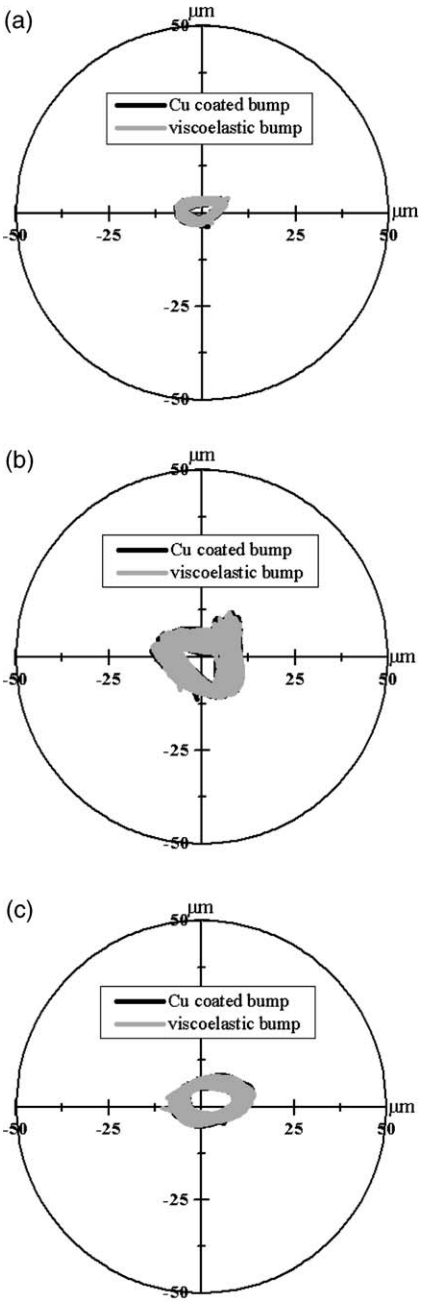

Fig. 9. Comparison of the vibration orbit between the bump and viscoelastic bearing at 20,000 RPM: (a) at the free end, (b) at the axial center, (c) at the turbine end.

structural damping of the VEFB has the dominant effect on suppression of rotor vibration. While the nonsynchronous orbit of the bump bearing occurs at 50,000 RPM, the nonsynchronous vibration of both bearings is much smaller than the synchronous vibration up to 40,000 RPM.

4. Conclusions and discussions

The ViscoElastic Foil Bearing (VEFB) is suggested in this paper. To demonstrate the superior characteristics,

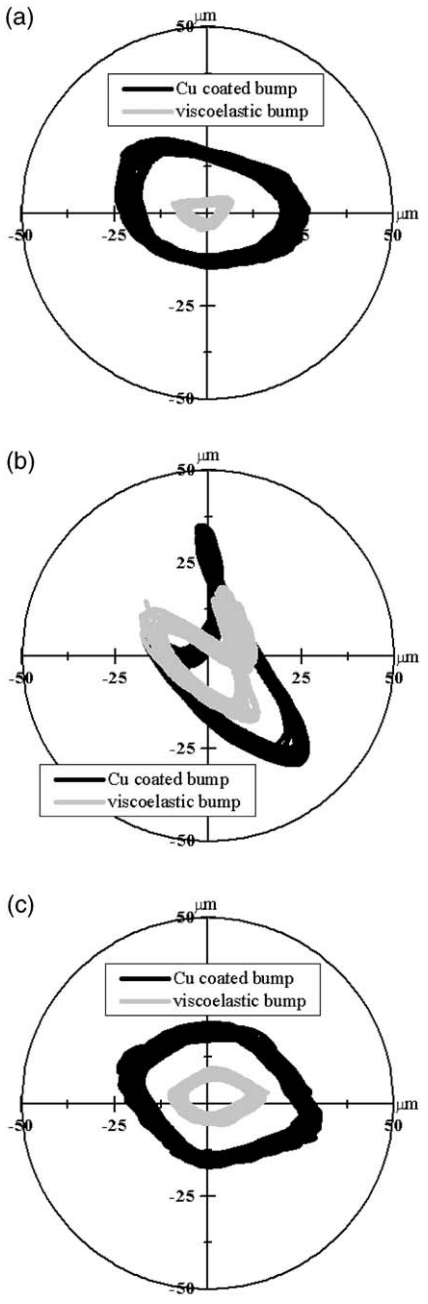

Fig. 10. Comparison of the vibration orbit between the bump and viscoelastic bearing at 30,000 RPM: (a) at the free end, (b) at the axial center, (c) at the turbine end.

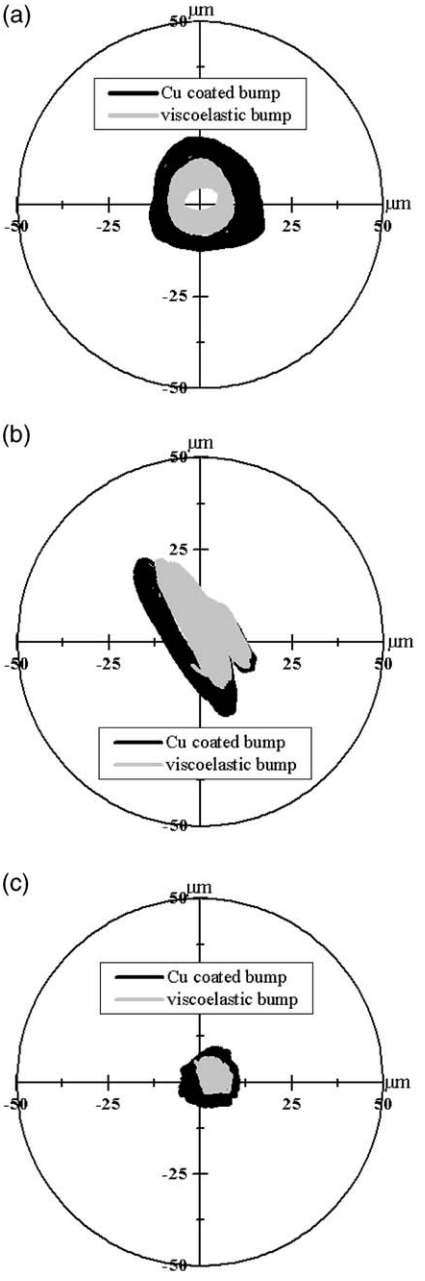

Fig. 11. Comparison of the vibration orbit between the bump and viscoelastic bearing at 40,000 RPM: (a) at the free end, (b) at the axial center, (c) at the turbine end.

super-bending-critical operation of the conventional bump foil bearing and the VEFB is examined, as well as the structural dynamic characteristics. In both tests, structural damping, vibration orbit, and the modal damping ratio of the bump bearing and the VEFB were compared. The structural dynamic test results show that the damping ratio is from 0.2 to 0.8 for a range of experiments while the structural dynamic stiffness of the VEFB is comparable or larger than that of the bump bearing. The results for super-bending-critical operation of the VEFB indicate that the enhanced structural damping of the viscoelastic foil dramatically reduces vibration near the bending critical speed. Thus, increased damping due to the viscoelasticity allows for suppression of the nonsynchronous orbit beyond the bending critical speed.

Acknowledgements

This work was supported by a grant from the Critical Technology 21 Project and the Dual Use Technology Program of the Ministry of Science and Technology, Korea.

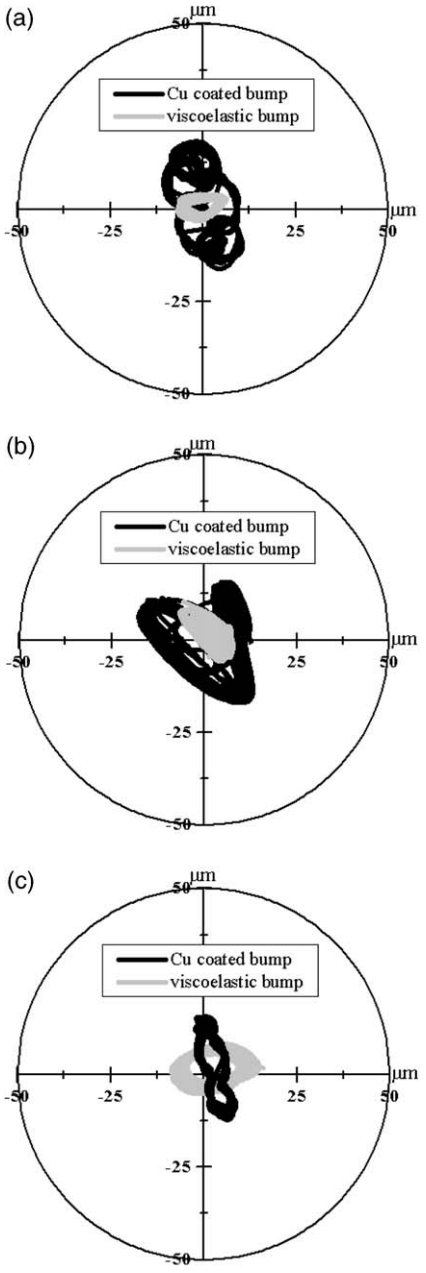

Fig. 12. Comparison of the vibration orbit between the bump and viscoelastic bearing at 50,000 RPM: (a) at the free end, (b) at the axial center, (c) at the turbine end.

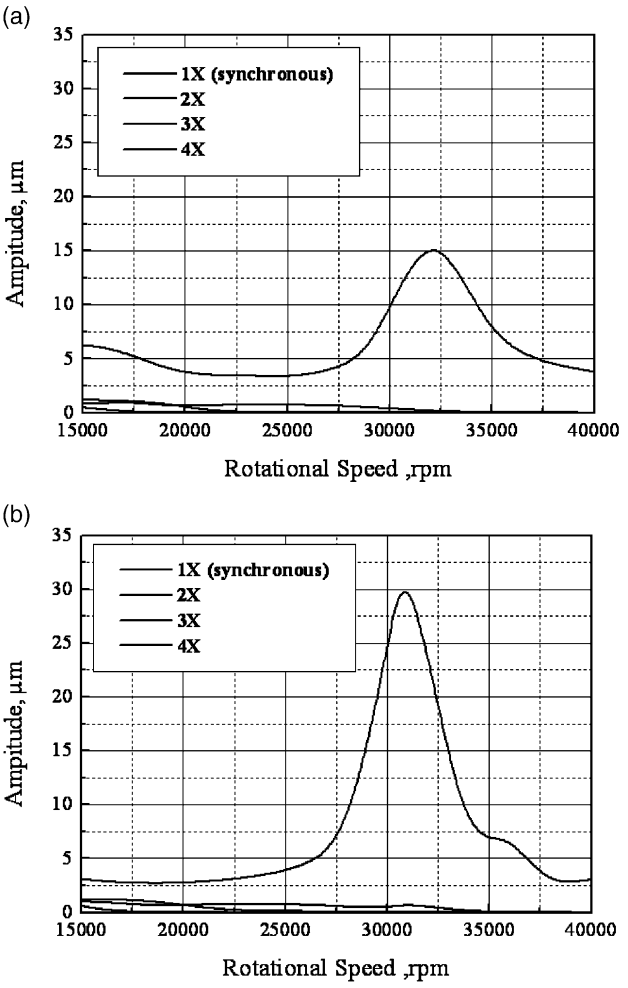

Fig. 13. Comparison of order plot between the bump bearing and the VEFB during speed-up: (a) viscoelastic bearing, (b) bump bearing.

Appendix A

The structural dynamic equation represents the relationships between the applied dynamic forces and the structural dynamic coefficients as follows.

$$\{K\} = [d]^{-1}(\{F\}-\{A\}) \tag{A1}$$

$\{K\}$,$\{F\}$, $\{A\}$, $[d]$ are dynamic coefficient, shaker-driven force, and housing acceleration vector, and system response matrix.

$$\{K\}^T = \{K_{yy},\ K_{yx},\ K_{xy},\ K_{xx},\ \Omega C_{yy},\ \Omega C_{yx},\ \Omega C_{xy},\ \Omega C_{xx}\} \tag{A2}$$

$$\{F\}^T = \{F_y,\ 0,\ 0,\ 0,\ 0,\ 0,\ F_x,\ 0\} \tag{A3}$$

$$\{A\}^T = M\Omega^2\{d_{yy}\cos\varphi_{yy},\ d_{yy}\sin\varphi_{yy},\ d_{yx}\cos\varphi_{yx},\ d_{yx}\sin\varphi_{yx},\ d_{xy}\cos\varphi_{xy},\ d_{xy}\sin\varphi_{xy},\ d_{xx}\cos\varphi_{xx},\ d_{xx}\sin\varphi_{xx}\} \tag{A4}$$

$$[d] = \begin{bmatrix} d_1 & d_3 & 0 & 0 & -d_2 & -d_4 & 0 & 0 \\ d_2 & d_4 & 0 & 0 & d_1 & d_3 & 0 & 0 \\ 0 & 0 & d_1 & d_3 & 0 & 0 & -d_2 & -d_4 \\ 0 & 0 & d_2 & d_4 & 0 & 0 & d_1 & d_3 \\ d_5 & d_7 & 0 & 0 & -d_6 & -d_8 & 0 & 0 \\ d_6 & d_8 & 0 & 0 & d_5 & d_7 & 0 & 0 \\ 0 & 0 & d_5 & d_7 & 0 & 0 & -d_6 & -d_8 \\ 0 & 0 & d_6 & d_8 & 0 & 0 & d_5 & d_7 \end{bmatrix} \tag{A5}$$

,

$$\begin{Bmatrix} d_1 \\ d_2 \\ d_3 \\ d_4 \\ d_5 \\ d_6 \\ d_7 \\ d_8 \end{Bmatrix} = \begin{Bmatrix} d_{yy}\cos\varphi_{yy} \\ d_{yy}\sin\varphi_{yy} \\ d_{yx}\cos\varphi_{yx} \\ d_{yx}\sin\varphi_{yx} \\ d_{xy}\cos\varphi_{xy} \\ d_{xy}\sin\varphi_{xy} \\ d_{xx}\cos\varphi_{xx} \\ d_{xx}\sin\varphi_{xx} \end{Bmatrix} \tag{A6}$$

where, K_{ij}, C_{ij} , F_i, Ω, d_{ij}, ϕ_{ij}, M are the structural stiffness and damping of bearing, shaker-driven force amplitude and frequency, amplitude and phase of the relative displacement between the housing and the shaft, and housing mass (i,j=x,y).

References

[1] Heshmat H. Operation of foil bearings beyond the bending critical mode. ASME J. of Tribology 2000;122:192–8.

[2] Dellacorte C, Valco M. Load capacity estimation of foil air journal bearings for oil-free turbomachinery application. ASME/STLE Tribology Conference in Seattle, Washington, Preprint No. 00-TC-4, 2000.

[3] Heshmat H, Shapiro W, Gray S. Development of foil journal bearings for high load capacity and high speed whirl stability. J. of Lubrication Technology 1982;104:149–56.

[4] Heshmat H, Roger Ku CP. Structural damping of self-acting compliant foil journal bearings. ASME J. of Tribolgoy 1994;116:76–82.

[5] Childs C. Turbomachinery Rotordynamics. New York: John Wiley & Sons, Inc, 1993.

[6] Adams Jr. ML. Rotating Machinery Vibration from Analysis to Troubleshooting. New York: Marcel Dekker, Inc, 2001.

[7] Ehrich FF. Handbook of Rotordynamics. McGraw-Hill, Inc, 1992.